⌘ *Author's Choice*

THE JOURNAL OF BIOLOGICAL CHEMISTRY VOL. 285, NO. 38, pp. 29406–29415, September 17, 2010

Crystal Structure of *Staphylococcus aureus* Metallopeptidase (Sapep) Reveals Large Domain Motions between the Manganese-bound and Apo-states*[S]

Received for publication, May 24, 2010, and in revised form, June 26, 2010 Published, JBC Papers in Press, July 7, 2010, DOI 10.1074/jbc.M110.147579

Tavarekere S. Girish and Balasubramanian Gopal[1]

From the Molecular Biophysics Unit, Indian Institute of Science, Bangalore 560 012, India

Proteases belonging to the M20 family are characterized by diverse substrate specificity and participate in several metabolic pathways. The *Staphylococcus aureus* metallopeptidase, Sapep, is a member of the aminoacylase-I/M20 protein family. This protein is a Mn^{2+}-dependent dipeptidase. The crystal structure of this protein in the Mn^{2+}-bound form and in the open, metal-free state suggests that large interdomain movements could potentially regulate the activity of this enzyme. We note that the extended inactive conformation is stabilized by a disulfide bond in the vicinity of the active site. Although these cysteines, Cys^{155} and Cys^{178}, are not active site residues, the reduced form of this enzyme is substantially more active as a dipeptidase. These findings acquire further relevance given a recent observation that this enzyme is only active in methicillin-resistant *S. aureus*. The structural and biochemical features of this enzyme provide a template for the design of novel methicillin-resistant *S. aureus*-specific therapeutics.

Staphylococcus aureus is the cause of most superficial infections of skin and soft tissues and life-threatening invasive infections like pneumonia, osteomyelitis, arthritis, endocarditis, and sepsis (1, 2). These cocci rapidly acquire resistance to several frontline antibiotics in both hospital as well as community settings (3). A genome-wide analysis reveals that subtle genetic changes can have a pronounced effect on the virulence of both methicillin-susceptible and methicillin-resistant *S. aureus* (MRSA)[2] (4). Rapid identification of MRSA strains is therefore crucial to alter the treatment regimen and for measures to prevent the spread of infection in a nosocomial setting. A recent report using activity-based protein profiling in *S. aureus* led to the identification of a novel resistance-associated dipeptidase that was noted to be selectively overexpressed in MRSA strains (5). Here, we describe the structure and biochemical features of this enzyme (NCBI ID, 3236055; KEGG ID, SACOL1801 subsequently referred to as Sapep) from an MRSA strain *S. aureus* spp. COL.

Sapep is a member of the M20 family of metalloproteases. These proteins catalyze a diverse range of reactions. Functional members of this class include *N*-acetylornithine deacetylase, succinyl-diaminopimelate desuccinylase, carboxypeptidase G2 (CPG2), and a tripeptidase, peptidase T (6). The structures of M20 proteases are remarkably well conserved despite poor sequence similarity. In general, these proteins adopt a two-domain structure and are either monomers or homodimers in solution. The only known exception is the aminopeptidase that has been characterized from *Aeromonas proteolytica* and *Streptomyces griseus* (7, 8). Of the two domains in M20 proteins, the first domain is referred to as the catalytic domain as it harbors residues essential for catalysis and metal binding. The second domain is referred to as the lid domain in monomeric M20 proteins (9) or as the dimerization domain in homodimeric enzymes (10–12). In either case, the active site is located between the two domains and contains a di-zinc center coordinated by residues from the catalytic domain. However, a few residues from the lid domain also play a role in substrate binding and catalytic activity (12, 13). Although most proteases of the M20 family bind either zinc or cobalt, manganese and magnesium are also preferred metal cofactors (14). An intriguing feature is the diversity of substrates hydrolyzed by these enzymes while retaining a similar active site conformation with identical metal-coordinating residues. A comparison of a substrate analogue-bound structure of *Lactobacillus delbrueckii* PepV (PepV) with two Zn^{2+} ions at the active site with the partially open structure of CPG2 from a *Pseudomonas* sp. led to the suggestion that variations in the interdomain arrangement between the catalytic and lid domains modulate the size of the active site cleft (9, 10). The ability of enzymes in the M20 family to act on diverse substrates has often been rationalized on the premise that the chemical reaction (amide hydrolysis) is retained in most cases, although the substrates are broadly similar in structure (15).

Although the catalytic mechanism has been well characterized for M20 metalloenzymes, the structural features that modulate function in this class of proteins remain less explored. A comparison between the substrate-bound and -free structures of the homodimeric β-alanine synthase suggested that conformational changes involving domain movements could poten-

* This work was supported in part by grants from the Department of Science and Technology and the Department of Biotechnology, Government of India.

⌘ *Author's Choice*—Final version full access.

[S] The on-line version of this article (available at http://www.jbc.org) contains supplemental Figs. S1–S3 and Table 1.

The atomic coordinates and structure factors (codes 3KHX, 3KHZ, and 3KI9) have been deposited in the Protein Data Bank, Research Collaboratory for Structural Bioinformatics, Rutgers University, New Brunswick, NJ (http://www.rcsb.org/).

[1] International Senior Research Fellow of the Wellcome Trust, United Kingdom. To whom all correspondence should be addressed. Tel.: 91-80-22933219; Fax: 9180-23600535; E-mail: bgopal@mbu.iisc.ernet.in.

[2] The abbreviations used are: MRSA, methicillin-resistant *S. aureus*; DTNB, 5,5′-dithiobis-(2-nitrobenzoic acid); TCEP, tris(2-carboxyethyl)phosphine; GdnHCl, guanidine hydrochloride; PEG, polyethylene glycol; Cd-ninhydrin method, cadmium-ninhydrin method; ITC, isothermal titration calorimetry; BisTris, 2-[bis(2-hydroxyethyl)amino]-2-(hydroxymethyl)propane-1,3-diol.

tially regulate the activity of these proteins (12). However, information on the inactive conformation in the case of monomeric M20 proteases remained elusive as the only monomeric structure known was of PepV in the active, substrate-bound form (9). Sapep shares 34.0% sequence identity with PepV and is a monomer in solution. The structure of Sapep in both the open and closed conformation described here suggests that large rearrangements between the catalytic and lid domains could potentially regulate this enzyme. A comparison of the inactive (open) and the active (closed) conformations further revealed a hitherto unanticipated mechanism by which the inactive conformation is stabilized. We note that the catalytic activity of Sapep was inhibited by a disulfide bond that stabilizes the open form under oxidizing conditions. This finding suggests that the inactive conformation of this protein could potentially be exploited for the development of selective inhibitors as in the case of the protein-tyrosine kinases (16).

MATERIALS AND METHODS

Cloning, Expression, and Purification of Recombinant Sapep—The gene (1.410 kb) encoding Sapep was PCR-amplified from the genomic DNA of *S. aureus* spp. COL using 5′ GTT CGC TAG CAT GTG GAA AGA AAA AGT TCA A 3′ and 5′ ACG CTC GAG TTA TTC CTC CAC GCA TAA TG 3′ as the forward and reverse primers, respectively. This gene was subsequently cloned into the pET15b bacterial expression vector between the NheI and XhoI restriction sites. 5′ CTT TTC GGT ATC AAC TTA GCA TAC CCA GAA GGA TTT GAA 3′ and 5′ TTC AAA TCC TTC TGG GTA TGC TAA GTT GAT ACC GAA AAG 3′ were used as the forward and reverse primers in a site-directed mutagenesis procedure to obtain the R350A variant of Sapep. The recombinant protein was expressed in BL21 (DE3) cells with a hexahistidine tag at the N terminus. 0.5 mM isopropyl β-D-1-thiogalactopyranoside was added to induce protein expression when the cell density reached an absorbance of 0.6 at 600 nm. Post-induction, the cells were grown at 17 °C for 8–10 h. Thereafter, these cells were harvested by pelleting at 6,000 rpm for 10 min. The cell pellet was resuspended in lysis buffer (50 mM Tris-HCl, pH 7.5, and 250 mM NaCl) and lysed by sonication. The supernatant from this stage was incubated with Ni^{2+}-NTA affinity beads (Sigma) for 1 h at 4 °C. The bound protein was eluted by a gradient of imidazole concentration from 5 to 200 mM in a buffer containing 50 mM Tris-HCl, pH 7.5, and 250 mM NaCl. Sapep was further purified on a Sephacryl S-200 gel filtration column equilibrated with 50 mM Tris-HCl, pH 7.5, 200 mM NaCl, and 1.0% glycerol to remove higher molecular weight contaminant proteins. The R350A Sapep mutant was purified using the same protocol. The Mn^{2+}-bound protein was also purified by the same procedure except that 3 mM tris(2-carboxyethyl)phosphine (TCEP) and 1.0 mM $MnCl_2$ were included in the purification buffers. Apo-Sapep was prepared by incubating the purified protein with 10 mM EDTA on ice for 5 h followed by dialysis for 24 h against a buffer containing 50 mM Tris-HCl, pH 7.5, 200 mM NaCl, and 10 mM EDTA. This step was followed by another dialysis step against the same buffer without EDTA.

Analytical Size-exclusion Chromatography—Both apo- and holo-Sapep were examined by analytical gel filtration chromatography on a Superdex S-200 gel filtration column (10/300 GL; GE Healthcare) using a UPC10 AKTA FPLC system (GE Healthcare). The buffer (25 mM Tris-HCl, pH 7.5, 125 mM NaCl) used in the case of holo-Sapep had 2.0 mM $MnCl_2$ with 10 mM TCEP, although that for apo-Sapep had 10 mM EDTA. 200 μl of 1 mg/ml each of apo- and holo-Sapep were passed through the column at a flow rate of 0.3 ml/min. Reduced apo-Sapep was obtained by incubating the apoprotein with 50 mM TCEP for about 5 h on ice.

Crystallization and Data Collection—Initial screening for the crystallization conditions was performed using crystallization kits, silicon oil, and paraffin oil from Hampton Research. The conditions were examined using both hanging drop (protein concentration at 5 mg/ml) and the sitting drop method under oil (protein concentration at 10.0 mg/ml) at 293 K, where the drop (4 μl) contained 2 μl of protein and 2 μl of the precipitating reagent solution. Initial crystals of the protein purified in the absence of Mn^{2+} were thin rod or needle-shaped micro-crystals in a condition containing 0.2 M ammonium acetate and diamond-shaped micro-crystals in a condition containing 1.8 M tri-ammonium citrate, pH 7.0. These conditions were subsequently modified to get diffraction quality crystals. The crystal that was used for data collection was obtained in a condition containing 0.2 M ammonium acetate, 0.1 M BisTris, pH 6.5, and 18.0% PEG 6000. Crystals of the R350A mutant were obtained in a condition containing 0.2 M ammonium sulfate, 0.2 M MES, pH 6.5, and 30.0% PEG Mono Methyl Ether 5000. Holo-Sapep was purified with Mn^{2+} and TCEP in the purification buffer and crystallized in a condition containing either magnesium acetate or calcium acetate. Crystals grown in magnesium acetate were further optimized to get diffraction quality crystals in a condition containing 0.2 M magnesium acetate tetrahydrate, 0.1 M sodium cacodylate, pH 6.8, and 22% PEG 8000. It was important to include excess of $MnCl_2$ and TCEP in the protein solution prior to crystallization trials to obtain diffraction quality crystals. All crystals were flash-frozen in liquid nitrogen using 10.0% glycerol as the cryoprotectant. All the diffraction data sets were processed using MOSFLM (17) and scaled using SCALA (18). The data collection and refinement statistics are reported in Table 1.

Crystal Structure Determination and Refinement—The structures were solved by molecular replacement using the program PHASER (19). Molecular replacement trials with the monoclinic data set using the PepV structure (Protein Data Bank code 1LFW; 34.0% sequence identity with Sapep) as a model were not successful. However, a molecular replacement strategy using the catalytic and lid domains of PepV as independent search models led to a successful structure solution with a log likelihood gain of 300. The model was subsequently refined using Refmac5 (20), and the fit of the model to the electron density was evaluated by COOT (21). It was important to use TLS restraints to achieve convergence in refinement. The structures of the catalytic and lid domains determined for Sapep in the open form were subsequently used as initial search models in the molecular replacement calculations for the closed form as well as the R350A mutant.

TABLE 1
Summary of data collection and refinement statistics

	PDB code 3KHX (open)	PDB code 3KHZ (R350A mutant)	PDB code 3KI9 (closed)
Data collection			
Wavelength	0.98 Å	1.5418 Å	1.5418 Å
Resolution	2.30 (2.42 to 2.30)	2.50 (2.64 to 2.5)	2.9 (3.06 to 2.9)[a]
Space group	$P2_1$	$P2_1$	*I*23
Unit cell dimensions	a = 64.82 Å b = 134.17 Å c = 68.28 Å β = 94.52°	a = 64.75Å b = 133.52 Å c = 67.71Å β = 95.59°	$a = b = c$ = 158.15 Å
No. of observations	185,172 (27,397)	337,344 (47,881)	116,012 (16,641)
Number of Unique Observations	51,315 (7488)	39,597 (5730)	14,758.0 (2141)
Mean I/σ(I)	14.8 (3.2)	20.9 (4.9)	14.2 (3.6)
Multiplicity	3.6 (3.7)	8.5 (8.4)	7.9 (7.8)
Completeness	99.4 (99.6)	100.0 (100.0)	100.0 (100.0)
R_{merge}[b]	7.1% (35.4%)	6.8% (41.4%)	10.8% (56.3%)
Refinement			
R_{work}[c]	24.7%	20.7%	20.21%
R_{free}[d]	27.7%	26.9%	26.26%
Model statistics			
No. of residues	846	868	466
No. of water molecules	182	113	26
r.m.s.d.[e] bond length	0.009 Å	0.011 Å	0.005 Å
r.m.s.d. bond angle	1.246°	1.350°	0.937°

[a] Values for outer shells are given in parentheses.
[b] $R_{merge} = \Sigma_j|\langle I\rangle - I_j|/\Sigma\langle I\rangle$, where I_j is the intensity of the jth reflection and $\langle I\rangle$ is the average intensity.
[c] $R_{work} = \Sigma_{hkl}|F_o - F_c|/\Sigma_{hkl}|F_o|$.
[d] R_{free} was calculated as for R_{work} but with 5% of the data excluded from the refinement calculation.
[e] r.m.s.d. is root mean square deviation.

Measurement of Peptidase Activity by the Cd-Ninhydrin Method—The dipeptidase activity of Sapep was measured using the Cd-ninhydrin method (22). In this colorimetric assay, various concentrations of the Phe-Val dipeptide substrate ranging from 0.125 to 4.0 mM were added to the reaction mixture containing 25 mM Tris-HCl, pH 7.5. The microcentrifuge tubes containing different concentrations of the Phe-Val dipeptide substrates were preincubated at 37 °C for 10 min. The peptidase reactions were initiated by adding 5 μl of the appropriately diluted enzyme into a total reaction volume of 100 μl. The reaction mixture was further incubated at 37 °C in a rotating shaker incubator for 30 min. The reaction was stopped by adding Cd-ninhydrin reagent. This solution was then heated at 84 °C for 10 min. The reaction was monitored by measuring the absorbance at 507 nm. A standard plot corresponding to calibrated amounts of Phe and Val amino acids was used as a reference. The kinetic parameters were calculated by a nonlinear least squares fit of the data using Origin software (OriginLab Co.). For determining metal-cofactor preferences for peptidase activity, apo-Sapep was incubated with various divalent metal ions. The regeneration of peptidase activity in response to a reducing agent was examined using the apoenzyme incubated with 2.0 mM $MnCl_2$ in the presence of 3.0 mM TCEP.

Analysis of Sulfhydryl Groups in Sapep—5 μM apo-Sapep was denatured by incubation with 7 M guanidine hydrochloride (GdnHCl) at room temperature for 1 h. The free thiol content was determined by adding 1000-fold molar excess of Ellman's reagent and monitoring the absorbance at 412 nm. An extinction coefficient of 13,700 cm^{-1} M^{-1} for the thionitrobenzoate anion was used to calculate the number of free sulfhydryl groups under denaturing conditions. To determine the total number of sulfhydryl groups in the reduced apoenzyme, 5 μM apo-Sapep was incubated with 10 mM TCEP at room temperature for 4 h and passed through a desalting column (NAP10; Amersham Biosciences) prior to the reaction with Ellman's reagent. For mass spectrometric analysis, DTNB-labeled proteins from the reaction mixture were further passed through a desalting column equilibrated with 10.0 mM ammonium bicarbonate buffer and were subsequently analyzed on a LC-ESI mass spectrometer (Bruker Daltonics, Inc.).

Isothermal Titration Calorimetry of Mn^{2+} Binding to Sapep—All the isothermal titration calorimetry (ITC) experiments were carried out in a VP-ITC microcalorimeter (MicroCal, Inc.) at 25 °C. The Sapep sample used in these experiments was dialyzed against 25 mM HEPES, pH 7.5, and 200 mM NaCl. The ligand ($MnCl_2$) solution for the titration was prepared in the final dialysis buffer. In this experiment, the sample cell (1.4 ml) was filled with 35 μM protein, and the ITC syringe (volume 298 μl) was loaded with 5 mM of the $MnCl_2$ solution. Titrations were performed by a stepwise addition of 5 μl of ligand solution into the sample cell. A time interval of 180 s between successive injections and a stirring speed of 307 rpm was maintained throughout the titration. The enthalpy, binding constant (K_b), and stoichiometry of ligand binding were determined by a nonlinear least square fit of the data using Origin software. The change in entropy (ΔS) was obtained using the equation ($\Delta G = \Delta H_b - T\Delta S$), where $\Delta G = -RT \ln K_b$.

RESULTS

Crystal Structure of the Open and Closed Conformations of Sapep—Crystals of Sapep in the open conformation were obtained when no metal ions were included in the protein purification process and in the crystallization solutions. In the open conformation, the catalytic and lid domains adopt an elongated arrangement with dimensions 46.16 × 100.28 × 50.21 Å (Fig. 1*a*). The Mn^{2+}-bound (closed) conformation, on the other hand, is more ellipsoidal in shape with the dimensions 55 × 84 × 54 Å. Two Mn^{2+} ions and a phosphate ion could be mod-

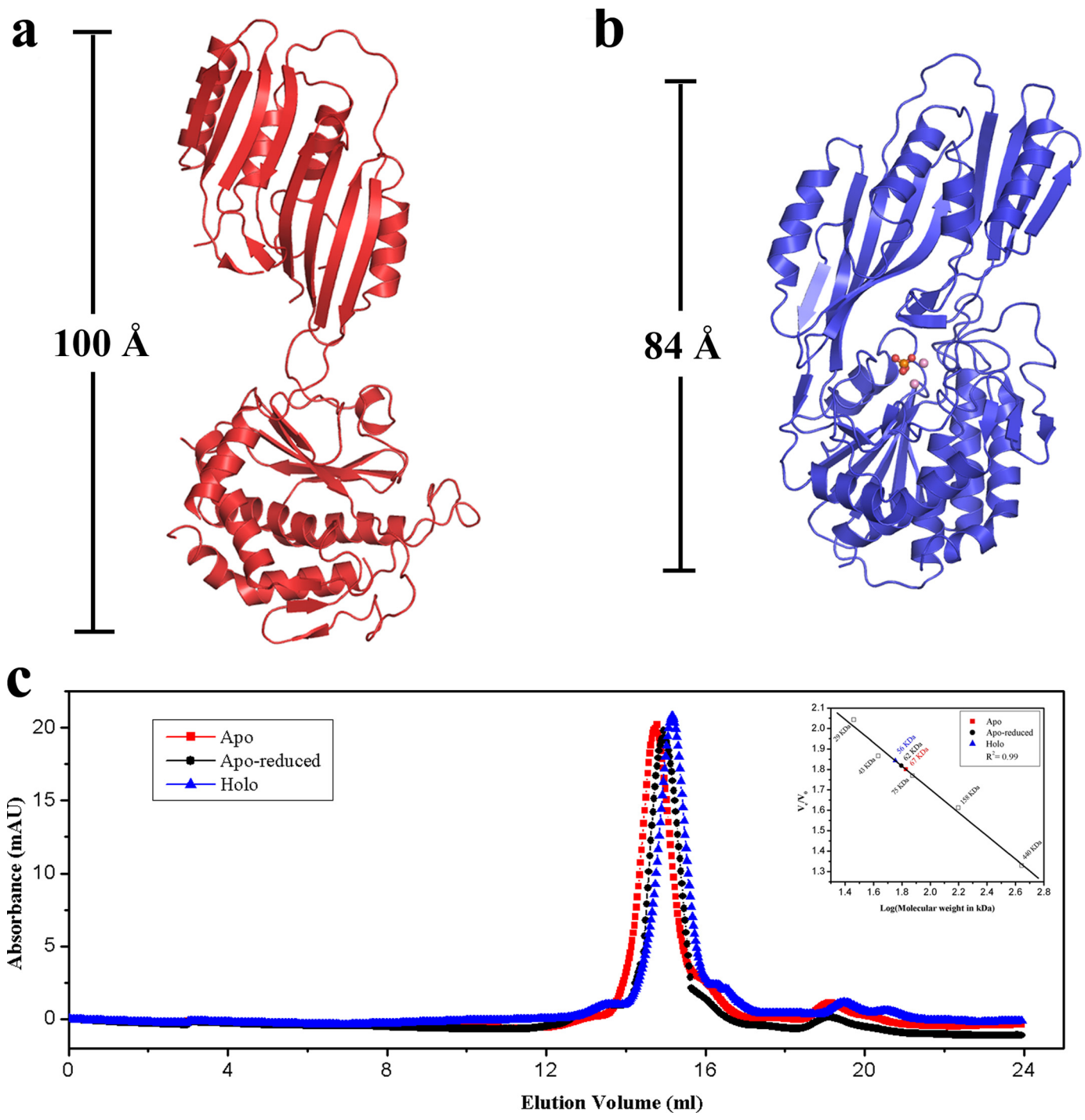

FIGURE 1. **Structure of the open and closed form of Sapep.** *a,* open form. Sapep does not bind metal ions in this conformation. *b,* closed form. The two Mn^{2+} bound at the active site are shown as *spheres,* although a bound phosphate ion is shown by a *ball and stick* representation. The dimensions of Sapep in the open and closed conformations were calculated using PDB SET (18). *c,* size-exclusion chromatography profiles suggest that the shape of Sapep in the apo- (*red*) and holo (*blue*)-form is different both in the crystal and in solution. The reduced form of apo-Sapep (*black*) also shows a slight shift in the elution volume compared with oxidized apo-Sapep. mAU, milliabsorbance units.

eled at the active site (Fig. 1*b*). The similarity of the closed form with the structure of the substrate-bound form of PepV suggests that this form corresponds to the active state of Sapep. In this conformation, the catalytic and the lid domains interact resulting in a buried surface area of about 500 $Å^2$ (Fig. 1*b*). The structures of the catalytic and lid domains are largely conserved in the two conformations, including a non-proline *cis*-peptide bond between Asp^{115} and Asp^{116} in both conformers. That the orientation of the domains in the open conformation is not a crystallization artifact was evident from the structure of Sapep solved in a different space group. The arrangement between the catalytic and lid domains in the trigonal crystal form of Sapep is identical to that solved using data from crystals in the monoclinic space group, although the crystal packing is different in these two crystal forms (data not shown). This domain arrangement corresponding to the open form was also seen in the

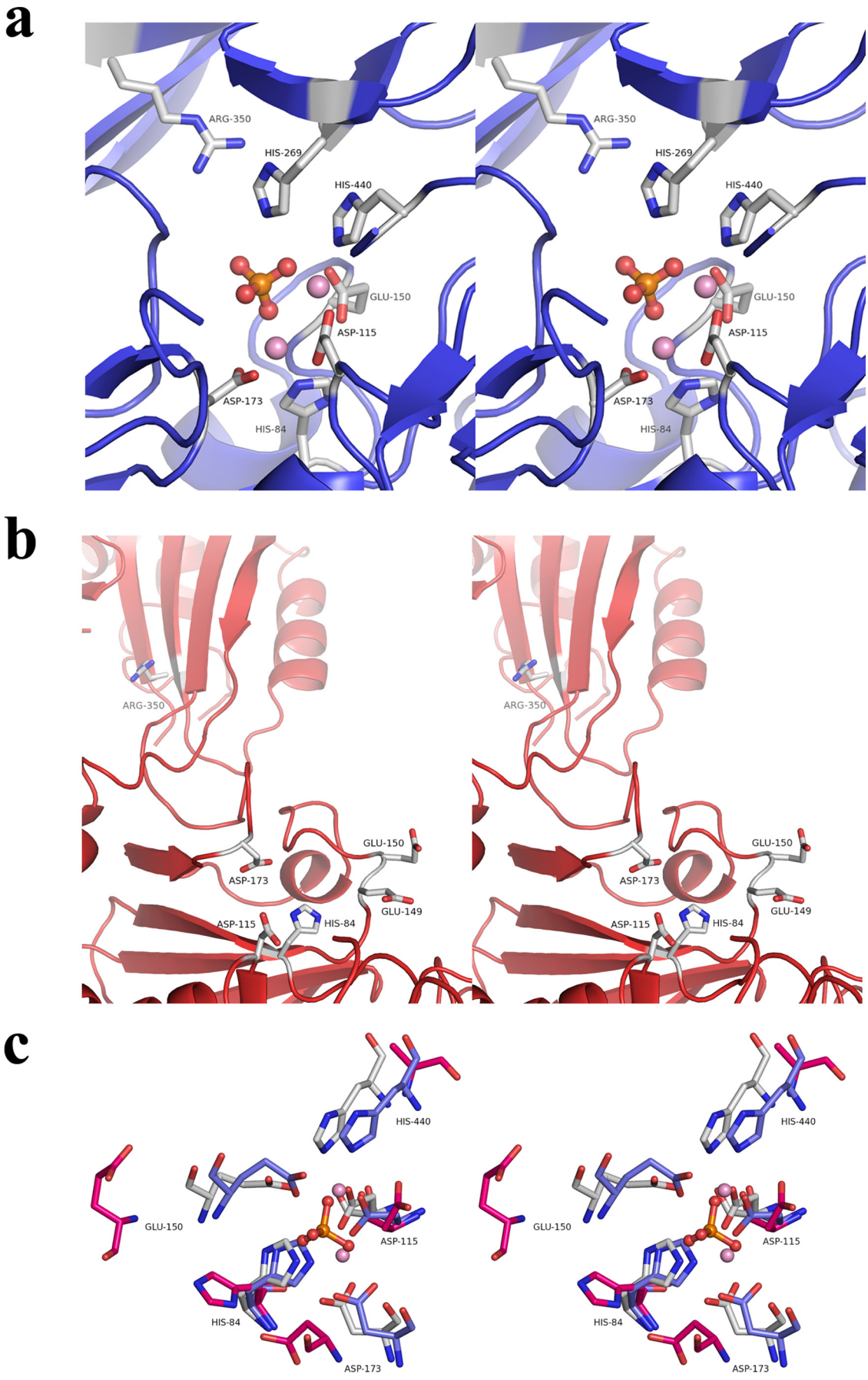
a
ARG-350
HIS-269
HIS-440
GLU-150
ASP-115
ASP-173
HIS-84
ARG-350
HIS-269
HIS-440
GLU-150
ASP-115
ASP-173
HIS-84
b
ARG-350
GLU-150
ASP-173
GLU-149
ASP-115
HIS-84
ARG-350
GLU-150
ASP-173
GLU-149
ASP-115
HIS-84
c
HIS-440
GLU-150
ASP-115
HIS-84
ASP-173
HIS-440
GLU-150
ASP-115
HIS-84
ASP-173

structure of the R350A mutant. The difference in the domain arrangement between the catalytic and lid domains is consistent with the solution data on Sapep in these two forms. Sapep is a monomer in both the open and closed forms. In a size-exclusion chromatography experiment, the Mn^{2+}-bound protein elutes at 15.2 ml on a Superdex S-200 column. This corresponds to a molecular mass of 56,000 Da. The apoprotein elutes at 14.8 ml, with the calculated mass corresponding to 67,000 Da. This change in the elution volume between the metal-free and Mn^{2+}-bound conformations of *S. aureus* peptidase suggests that the differences noted in the domain arrangement between the open and closed form also exist in solution (Fig. 1*c*).

The overall structure of the catalytic domain is similar in both the open and closed forms of Sapep barring two stretches of the polypeptide chain that assume different conformations. β8 is an extended polypeptide, although α4 is a shorter helix in the open form. Residues 320–327 and 404–440 (β9) could not be modeled in the open form due to poor electron density. The catalytic domain has a α/β fold comprising residues 1–181 and 387–469. Seven of the 10 β-strands form a large central β-sheet with the strands arranged in the order β1-β2-β6-β3-β7-β9-β8. β2 is the only anti-parallel β-strand in this arrangement. The remaining strands β4, β5, and β10 form a β-sheet. Five of the six helices (α4 is an exception) pack on the front side of a large β-sheet. The lid domain, comprising residues 182–388, also has an α/β fold. Twelve β-strands are distributed between three β-sheets, of which a flat major sheet contains eight anti-parallel β-strands arranged in the order β′11-β′1-β′10-β′9-β′2-β′4-β′6-β′5. The lid domain also shows a few changes in the secondary structure between the open and closed forms. Residues 384–386 that form a strand (β′12) in the closed form adopt an extended conformation in the open form of Sapep. Because of poor electron density, residues 320–327 (β′8) could not be modeled in the open form. Another crucial difference between the two forms of Sapep is the presence of a disulfide bridge between Cys^{155} and Cys^{178} in the open form.

Active Site Cavity—The crystal structure of the closed form of Sapep reveals an active site that is similar to that of PepV. This similarity is most prominent at the bottom of the active site cleft formed by the so-called Gly bulge comprising Gly^{414}–Gly^{415}–Gly^{416}–Thr^{417}. As is the case in other M20 peptidases, it is possible to define a front and a back end to the active site. The back end of the active site is lined by residues Lys^{379}, Val^{380}, and Gln^{381} of the catalytic domain and Gly^{184}, Ile^{185}, and Thr^{186} of the lid domain. The front end of the tunnel is formed by residues Leu^{438} and Met^{439}. Two Mn^{2+} ions could be modeled into the electron density at the active site. One Mn^{2+} ion is coordinated by the side chains of Asp^{115}, Glu^{150}, and His^{440}, although the other is coordinated by His^{84}, Asp^{115}, and Asp^{173} (Fig. 2). The two Mn^{2+} ions are located at a distance of 3.5 Å from each other. Although all the metal-coordinating residues are from the catalytic domain, the orientation of the side chains of His^{269}, Arg^{350}, and Asn^{216} in the lid domain also appear to substantially influence metal co-factor binding in the closed conformation.

The orientation between the catalytic and the lid domains in the open conformation of Sapep minimizes the interaction between these domains. Although the side chains of residues that coordinate the Mn^{2+} ions in the open form, *viz.* His^{84}, Asp^{115}, Asp^{173}, and Glu^{150} are well defined in electron density, they adopt a different rotamer to that seen in the closed form (Fig. 2). Indeed, no density for a metal ion was located in the vicinity of these residues. Because of poor electron density, the residues of the Gly bulge, which form the S1 subsite of the active site cleft, could not be modeled in the open conformation.

Transitions between the Open and Closed Forms Involve Local Changes in Secondary Structure Near the Hinge—The hinge segment in the catalytic domain includes the stretch between the residues Lys^{154}–Thr^{162} and Ala^{174}–Phe^{176} (Fig. 3). These two stretches of the polypeptide chain assume different conformations in the open and closed forms. In the closed form, residues Lys^{154}–Thr^{162} are a part of a long helix (α4), although α4 is much shorter (Arg^{158}—Thr^{162}) in the open structure. The other part of the hinge includes the stretch His^{384}–Val^{386} in the lid domain (Fig. 3). This segment is a β-strand (β′12) in the closed conformation and an extended loop in the open structure. The regions of the polypeptide chain that form the hinge segment are well defined in the electron density map in both the open and closed forms (supplemental Fig. S1). The localization of changes to the secondary structure elements in the hinge between the two domains suggests that these structural rearrangements facilitate large scale domain motions between the active and inactive conformations of this protein.

The swivel motion between the catalytic and lid domains in the open and closed forms was quantified considering Phe^{170} and Pro^{391} as pivots for interdomain movements. The axes were defined by using the center of mass of the catalytic and lid domains in the open and closed structures. The angle between the line joining the center of mass of the catalytic domain and the hinge and lid domain of each structure (α) corresponds to 141° in the open and 70° in the closed structure (Fig. 3). Thus, a rotation of 71° is traversed by the lid domain between the open and closed conformations.

Disulfide Clamp Stabilizes the Open Conformation—A comparison of the crystal structure of Sapep in the open and closed forms revealed the presence of a disulfide bond in the open conformer. Electron density for this disulfide bond was clearly seen between Cys^{155} and Cys^{178} in the open form of Sapep (Fig. 3). The major differences in the structure that facilitate this disulfide is the destabilization of helix α4 in the open form. Although the Cβ–Cβ distances between Cys^{155} and Cys^{178} are 3.9 Å in the open form, it stretches to 23.5 Å in the closed form. Both these Cys residues are free in the crystal structure of the closed form. Subsequent biochemical analysis clearly demon-

FIGURE 2. **Active site of Sapep.** Stereo view of the active site in the closed form (*a*) and the open form (*b*). The residues that are important for metal coordination and catalysis are shown by *sticks*. *c*, superposition of the active site regions of Sapep in the apo (*red*), Mn^{2+}-bound (*blue*), and PepV from *L. delbrueckii* (*silver*). The active site of the closed form of Sapep is similar to that of PepV.

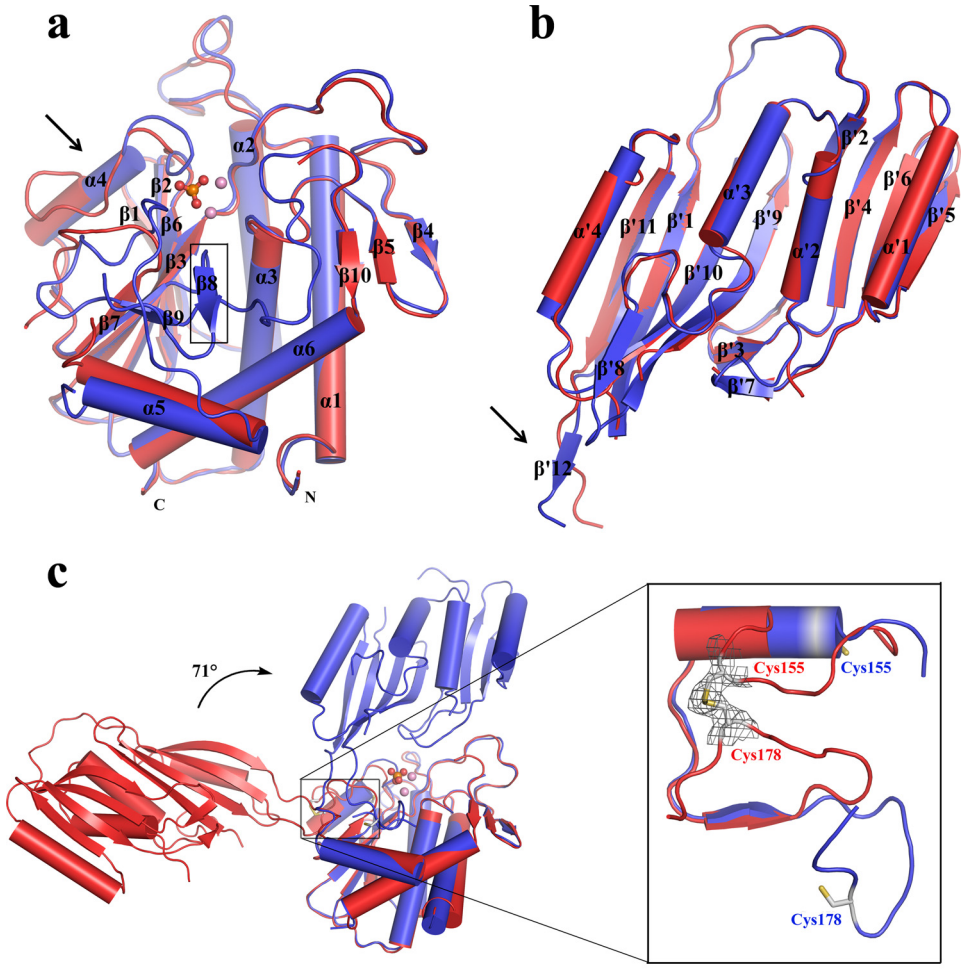

FIGURE 3. **A disulfide bond stabilizes the open conformation of Sapep.** Comparison between the catalytic (*a*) and the lid (*b*) domains of the open and closed forms of Sapep. The regions of polypeptide chain that assume different conformations are *highlighted*. The electron density for residues in the hinge region between the catalytic and lid domains is shown in supplemental Fig. S1. *c*, structural superposition of the open (*red*) and closed form (*blue*). A rotation of 71° was calculated between the open and closed conformations. The *inset* shows a $2mF_o - DF_c$ electron density map (at 1.0σ level) at the location of the disulfide bond between Cys^{155} and Cys^{178} in the open form. The mass spectroscopic analysis confirming this structural information is shown in supplemental Fig. S2.

TABLE 2

List of dipeptides hydrolyzed by Sapep

+ indicates mild hydrolysis; ++ indicates moderate hydrolysis, and +++ indicates highly hydrolyzed. Note: dipeptidase activity for Sapep was screened using a TLC-based assay. In this assay, 10 μl of dipeptide (5.0 mg/ml) was incubated with 2 μg of the enzyme in 50 mM Tris-HCl buffer, pH 7.5 (at 37 °C for 30 min). The hydrolysis was monitored by running 5 μl each of the reaction mixture on a silica-coated TLC plate using ethanol/acetic acid (90:10) solvent mixture as the mobile phase. The spots were visualized by spraying 1.0% ninhydrin in acetone.

Dipeptide	Activity
Gly–L-Lys	+
Gly–L-Ser	+
L-Ala–L-Ser	+
L-Asp–L-Lys	+
L-His–L-Leu	+
L-Lys–L-Phe	++
L-Lys–L-Leu	++
L-Ser–L-His	++
L-Phe–L-Val	+++
L-Phe–L-Leu	+++
L-Arg–L-Ala	+++
L-Arg–L-Val	+++
L-Arg–L-Leu	+++
L-Arg–L-Ile	+++

strated the presence of this disulfide in the apo-form of this protein. Two experiments, one using DTNB labeling and the other involving mass spectrometric analysis, were consistent with the crystallographic observation of a disulfide bond in the apo-form of Sapep. In the DTNB labeling experiment, 5 μM of the protein was denatured in 7 M GdnHCl and was subsequently incubated with 1000-fold molar excess of Ellman's reagent. From the absorbance measured at 412 nm, two free thiol groups were inferred in the case of apo-Sapep. The experiment with the reduced protein revealed all four Cys residues in the protein. For mass spectrometric analysis, 5 μM of the apoprotein was denatured in 7 M GdnHCl and incubated with 1000-fold molar excess of DTNB. This labeled protein corresponded to a mass of 55,769 Da (consistent with an addition of two DTNB molecules to Sapep (55,373 Da)) (supplemental Fig. S2).

Functional Characterization of Sapep—Functional predictions based on conserved sequence features suggested Sapep to be an M20 peptidase and a succinyl-diaminopimelate desuccinylase involved in L-lysine biosynthesis. The substrate specificity for the dipeptidase activity of Sapep was characterized using a library of dipeptides (supplemental Table 1). A sub-set of these dipeptides was hydrolyzed by Sapep with marginal variation in catalytic efficiency. Sapep could thus be described as a nonspecific peptidase (Table 2). The dipeptidase activity of Sapep is thus similar to that of *Salmonella enterica* DapE (15). The kinetic parameters for dipeptidase activity was further characterized using a dipeptide Phe-Val. The hydrolysis of the dipeptide was monitored by a colorimetric assay using the Cd-ninhydrin method (Fig. 4*a*). In an effort to identify the ideal metal cofactor for dipeptidase activity, assays were performed by incubating the apoenzyme in the presence of different metal ions. We note that apo-Sapep incubated with 2 mM $MnCl_2$ in 25 mM Tris-HCl, pH 7.5, is most suited for dipeptidase activity (Fig. 4*b*). Mn^{2+} binding to Sapep was also monitored by ITC (Fig. 4*c*). The structural similarity of Sapep with the dipeptidase PepV prompted an examination of the role of residues in the lid domain on the catalytic activity of this protein. In the crystal structure of PepV, a residue from the lid domain Arg^{350} forms part of the active site (9). This residue is proposed to be important in stabilizing the bound carboxylate group of peptide substrate. In the open form of

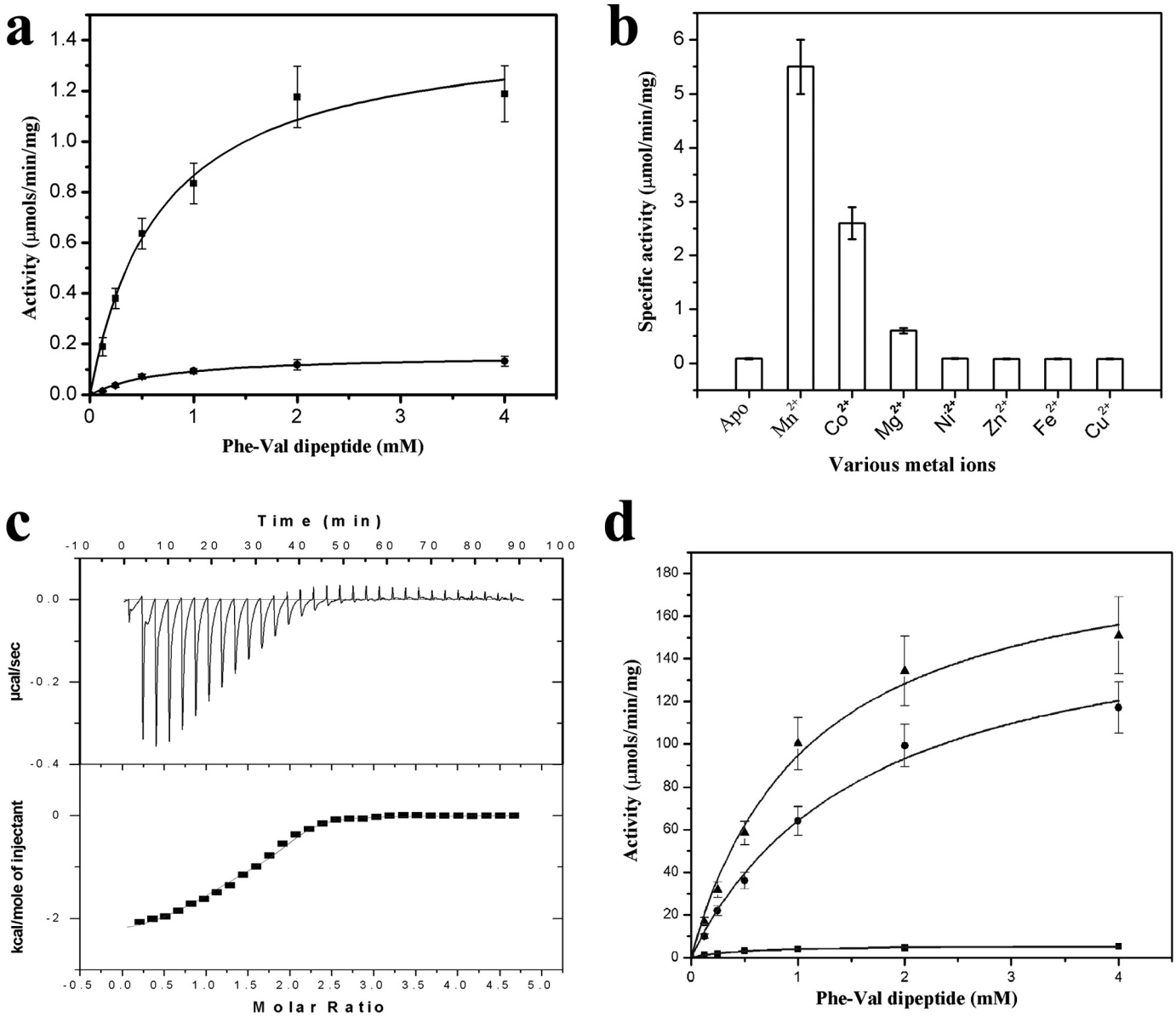

FIGURE 4. **Sapep is a Mn^{2+} dipeptidase.** *a,* data for Phe-Val dipeptide hydrolysis by wild type Sapep (■) and the R350A mutant (●) could be fitted into Michaelis-Menten kinetics. The assay was carried out with the Sapep sample that crystallized in the open conformation. The low k_{cat} value (1.3 ± 0.18 s^{-1}) calculated for the wild type Sapep suggests that a major fraction of the purified protein was in the inactive form. The R350A mutant of Sapep shows significant reduction in catalytic activity (k_{cat} = 0.15 ± 0.01 s^{-1}). The assay buffer contained 25 mM Tris-HCl, pH 7.5. *b,* regeneration of the catalytic activity of apo-Sapep by incubation with different metal co-factors. Maximum peptidase activity was seen in the case of Mn^{2+} followed by Co^{2+} and Mg^{2+}. This assay was performed with a Phe-Val dipeptide as substrate using the Cd-ninhydrin method (22). *c,* Mn^{2+} binding to Sapep was confirmed by isothermal titration calorimetry. The *top panel* shows the heat exchanged during Mn^{2+} binding to Sapep, and the *bottom panel* shows the least square fit of the data. The data could be fitted into a sequential binding model with $n = 2$. The binding constants calculated from the fit are $K_{b1} = 6.067 \times 10^6 \pm 2.01 \times 10^6$ M^{-1} and $K_{b2} = 7.773 \times 10^5 \pm 1.674 \times 10^5$ M^{-1}. *d,* regeneration of peptidase activity is sensitive to reducing agents. In this experiment, apo-Sapep was incubated with 2 mM $MnCl_2$ in an assay buffer containing 25 mM Tris-HCl, pH 7.5, with 3 mM TCEP. The regenerated activity of apoprotein without reducing agent (■) is ~10% that of freshly purified holo-Sapep, although samples with a reducing agent (●) are about 85.0% as active as the holo-protein (▲).

Sapep, the side chain of Arg^{350} is oriented (about 34 Å) away from the catalytically important Glu^{149}. The necessity of lid closure for catalytic activity was clear by the significant reduction in activity in the R350A mutant of Sapep (Fig. 4*a* and supplemental Fig. S3). It therefore appeared likely that decreasing the restraints between the movements between the catalytic and lid domains would increase the catalytic efficiency of this enzyme. A prominent restraint that could be deduced based on the crystal structure was that of a disulfide bond that stabilizes the open, inactive conformation of this enzyme. This hypothesis was examined by the addition of the reducing agent TCEP in the reaction condition. The regenerated activity of apo-Sapep incubated with 3 mM TCEP and 2 mM $MnCl_2$ in the assay buffer was significantly higher when compared with the apoenzyme incubated with 2 mM $MnCl_2$ alone (Fig. 4*d* and Table 3). We note that the K_m value varies substantially in these assays. The likely cause for this fluctuation could be the low catalytic activity of the enzyme in oxidizing conditions along with errors due to the marginal sensitivity of the Cd-ninhydrin method. Nonetheless, it appears likely that the disulfide bond seen in the open form of

TABLE 3
Kinetic parameters of the peptidase activity of Sapep

Protein	K_m	k_{cat}	Relative activity
	mM	s^{-1}	%
Sapep	0.67 ± 0.10	1.3 ± 0.18	0.70
Sapep + Mn^{2+}	1.15 ± 0.12	55.5 ± 4.6	30.0
Sapep + Mn^{2+} + TCEP	1.10 ± 0.10	185.0 ± 16	100.0
Apo-Sapep + Mn^{2+}	0.52 ± 0.12	5.5 ± 0.55	3.0
Apo-Sapep + Mn^{2+} + TCEP	1.64 ± 0.22	157.0 ± 14.0	85.0

Sapep stabilizes the inactive conformation of this enzyme resulting in low peptidase activity under oxidizing conditions.

DISCUSSION

Enzymes of the M20/aminoacylase-1 family perform diverse metabolic functions and have thus attracted much attention both from the perspective of protein engineering as well as for their potential as targets for the design of antibiotics. Prominent examples include the inhibition of human serum carnosinase in the treatment of diabetes and homocarnosinosis (23), and carboxypeptidase G2 as a rescue agent in cases of methotrexate overdose (10, 24). Sapep belonging M20/aminoacylase-1 family is reported to be active only in MRSA and absent in methicillin-susceptible *S. aureus* (5), thus representing an important target for the design of novel MRSA-specific agents.

The first structure of Sapep to be determined had the open conformation of this enzyme. This appeared surprising as the catalytic and lid domains were stretched in an elongated arrangement. However, the observation that mutating a putative active site residue (R350A) in the lid domain resulted in significantly lower catalytic activity clearly showed that Sapep is similar to other M20 peptidases that utilize both catalytic and lid domains. This finding thus suggested that large domain motions in Sapep could regulate the activity of this enzyme. Freshly purified wild type Sapep had rather poor catalytic activity with a low k_{cat} value (1.3 ± 0.18 s^{-1}). The enzymatic activity improved by ~200-fold upon the addition of Mn^{2+} and a reducing agent. This biochemical observation allowed us to crystallize this peptidase in the closed metal-bound form.

A rotation of 71° was observed for the lid domain between the open (inactive) and the closed (active) conformations of Sapep (Fig. 3*c*). Such large movements of the lid domain appear to be facilitated by changes in the secondary structure elements of both catalytic and lid domains near the hinge (Fig. 3, *a* and *b*). The interdomain motions observed between the Mn^{2+}-bound and metal-free Sapep not only reveal how variability in the active site cleft could be achieved but also provide a structural basis for the inactivation of this enzyme. The structure of Sapep thus suggests that monomeric M20 proteases are similar to the dimeric aminoacylases whereby large domain motions govern enzymatic activity.

Sapep appears to be only active in MRSA strains (5). This protein could thus be potentially used as a biomarker for resistant *S. aureus* strains. Conventional strategies to detect MRSA rely on the detection of the protein PBP2a, coded by the *mecA* gene, at either the DNA or protein levels (25). This strategy, however, fails to detect MRSA strains that lack the *mec* cassette, a plasmid-encoded gene cassette containing *mecA* (26, 27). The crystal structure and biochemical characteristics of this enzyme now provide a template for the rational design of biomarkers for MRSA as well as new MRSA-specific therapeutic strategies. Although many M20 proteases are important drug targets, the similar overall structure and active site geometry of these proteins have been a limiting factor in the design of specific inhibitor molecules. The structural features of the open conformation of Sapep suggest a template that can be utilized in the design of specific ligands that bind this enzyme. The widely used cancer drug ST1–571 (also known as imatinib), for example, functions by stabilizing the inactive conformation of Abelson protein kinase (Abl) and type III receptor protein-tyrosine kinase (c-Kit) (16).

CONCLUSIONS

The crystal structure of Sapep was determined in both the inactive (open) and the Mn^{2+}-bound (closed) forms. A comparison between these two structures revealed the presence of a disulfide bond between Cys^{155} and Cys^{178} in the open form. This finding, along with the observation that the peptidase activity of Sapep is substantially enhanced in the presence of reducing agents, suggests that this disulfide could inactivate this enzyme by stabilizing the open conformation. The biochemical and structural data on Sapep thus provide a template for the design of ligands that could selectively target this enzyme. The physiological significance of the observation that this protein is more active in reducing conditions remains to be explored, especially as it is seen to be substantially activated only in MRSA strains.

REFERENCES

1. Cunningham, R., Cockayne, A., and Humphreys, H. (1996) *J. Med. Microbiol.* **44,** 157–164
2. Maki, J. (1981) *Am. J. Med.* **70,** 714–732
3. Mwangi, M. M., Wu, S. W., Zhou, Y., Sieradzki, K., de Lencastre, H., Richardson, P., Bruce, D., Rubin, E., Myers, E., Siggia, E. D., and Tomasz, A. (2007) *Proc. Natl. Acad. Sci. U.S.A.* **104,** 9451–9456
4. Highlander, S. K., Hultén, K. G., Qin, X., Jiang, H., Yerrapragada, S., Mason, E. O., Jr., Shang, Y., Williams, T. M., Fortunov, R. M., Liu, Y., Igboeli, O., Petrosino, J., Tirumalai, M., Uzman, A., Fox, G. E., Cardenas, A. M., Muzny, D. M., Hemphill, L., Ding, Y., Dugan, S., Blyth, P. R., Buhay, C. J., Dinh, H. H., Hawes, A. C., Holder, M., Kovar, C. L., Lee, S. L., Liu, W., Nazareth, L. V., Wang, Q., Zhou, J., Kaplan, S. L., and Weinstock, G. M. (2007) *BMC Microbiol.* **7,** 99
5. Staub, I., and Sieber, S. A. (2009) *J. Am. Chem. Soc.* **131,** 6271–6276
6. Biagini, A., and Puigserver, A. (2001) *Comp. Biochem. Physiol. B Biochem. Mol. Biol.* **128,** 469–481
7. Chevrier, B., D'Orchymont, H., Schalk, C., Tarnus, C., and Moras, D. (1996) *Eur. J. Biochem.* **237,** 393–398
8. Greenblatt, H. M., Almog, O., Maras, B., Spungin-Bialik, A., Barra, D., Blumberg, S., and Shoham, G. (1997) *J. Mol. Biol.* **265,** 620–636
9. Jozic, D., Bourenkow, G., Bartunik, H., Scholze, H., Dive, V., Henrich, B., Huber, R., Bode, W., and Maskos, K. (2002) *Structure* **10,** 1097–1106
10. Rowsell, S., Pauptit, R. A., Tucker, A. D., Melton, R. G., Blow, D. M., and Brick, P. (1997) *Structure* **5,** 337–347
11. Håkansson, K., and Miller, C. G. (2002) *Eur. J. Biochem.* **269,** 443–450
12. Lundgren, S., Andersen, B., Piskur, J., and Dobritzsch, D. (2007) *J. Biol. Chem.* **282,** 36037–36047
13. Lindner, H. A., Lunin, V. V., Alary, A., Hecker, R., Cygler, M., and Ménard, R. (2003) *J. Biol. Chem.* **278,** 44496–44504
14. Munih, P., Moulin, A., Stamper, C. C., Bennett, B., Ringe, D., Petsko, G. A., and Holz, R. C. (2007) *J. Inorg. Biochem.* **101,** 1099–1107
15. Broder, D. H., and Miller, C. G. (2003) *J. Bacteriol.* **185,** 4748–4754

16. Schindler, T., Bornmann, W., Pellicena, P., Miller, W. T., Clarkson, B., and Kuriyan, J. (2000) *Science* **289,** 1938–1942
17. Leslie, A. G. (1992) *Joint CCP4 + ESF-EAMCB Newsletter on Protein Crystallography,* No. 26
18. Collaborative Computational Project No. 4 (1994) *Acta Crystallogr. D Biol. Crystallogr.* **50,** 760–763
19. Storoni, L. C., McCoy, A. J., and Read, R. J. (2004) *Acta Crystallogr. D Biol. Crystallogr.* **60,** 432–438
20. Murshudov, G. N., Vagin, A. A., and Dodson, E. J. (1997) *Acta Crystallogr. D Biol. Crystallogr.* **53,** 240–255
21. Emsley, P., and Cowtan, K. (2004) *Acta Crystallogr. D Biol. Crystallogr.* **60,** 2126–2132
22. Doi, E., Shibata, D., and Matoba, T. (1981) *Anal. Biochem.* **118,** 173–184
23. Janssen, B., Hohenadel, D., Brinkkoetter, P., Peters, V., Rind, N., Fischer, C., Rychlik, I., Cerna, M., Romzova, M., de Heer, E., Baelde, H., Bakker, S. J., Zirie, M., Rondeau, E., Mathieson, P., Saleem, M. A., Meyer, J., Köppel, H., Sauerhoefer, S., Bartram, C. R., Nawroth, P., Hammes, H. P., Yard, B. A., Zschocke, J., and van der Woude, F. J. (2005) *Diabetes* **54,** 2320–2327
24. Widemann, B. C., and Adamson, P. C. (2006) *Oncologist* **11,** 694–703
25. Katayama, Y., Ito, T., and Hiramatsu, K. (2000) *Antimicrob. Agents Chemother.* **44,** 1549–1555
26. Zhou, Y., Antignac, A., Wu, S. W., and Tomasz, A. (2008) *J. Bacteriol.* **190,** 508–514
27. Mongkolrattanothai, K., Boyle, S., Murphy, T. V., and Daum, R. S. (2004) *Antimicrob. Agents Chemother.* **48,** 1823–1836